

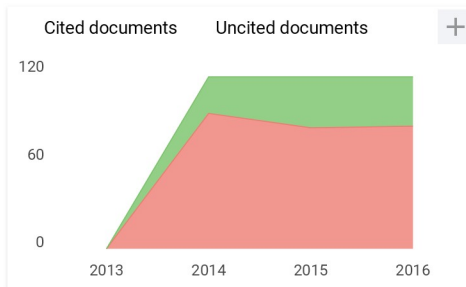
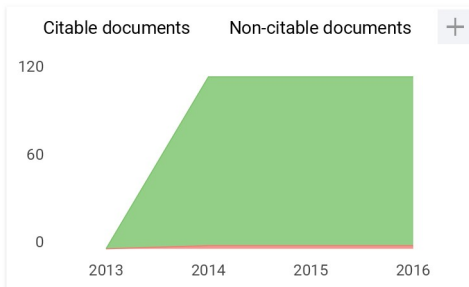
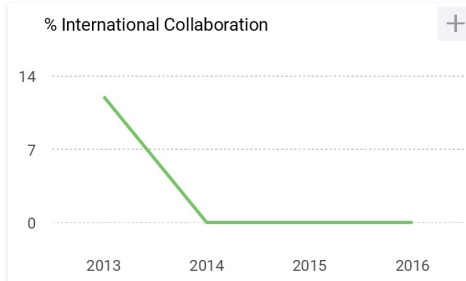
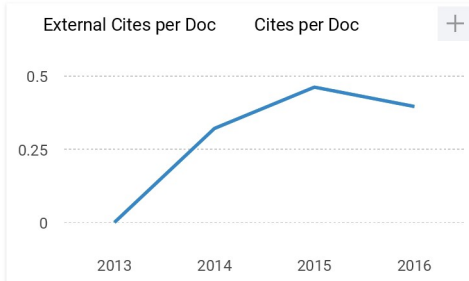
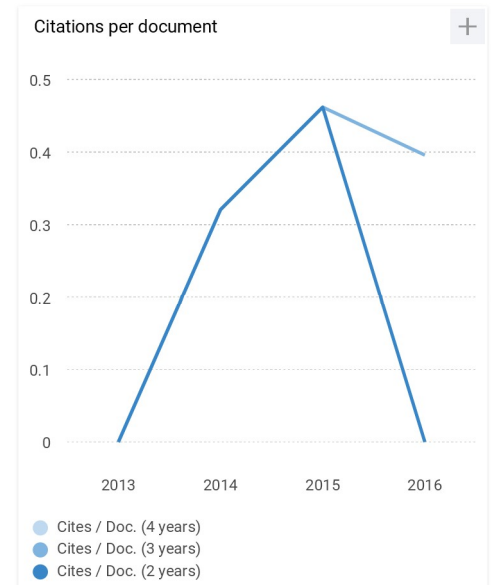
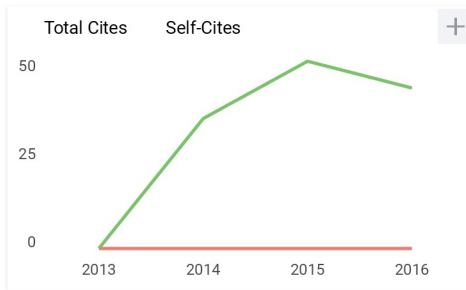
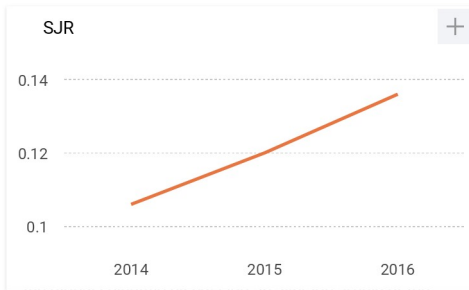


Proceedings - RSM 2013: 2013 IEEE Regional Symposium on Micro and Nano Electronics

Country	United States -  SJR Ranking of United States	<h1>7</h1> <p>H Index</p>
Subject Area and Category	Engineering Electrical and Electronic Engineering	
Publisher		
Publication type	Conferences and Proceedings	
ISSN	-	
Coverage	-	
	 Join the conversation about this journal	



Proceedings - RSM 2013: 2013 IEEE Regional...

Not yet assigned quartile

SJR 2019 

powered by scimagojr.com

← Show this widget in your own website

Just copy the code below and paste within your html code:

```
<a href="https://www.scim
```

Metrics based on Scopus® data as of April 2020

Leave a comment

Name

Email

(will not be published)

RSM 2013

**IEEE REGIONAL
SYMPOSIUM ON MICRO
AND NANO ELECTRONICS**

25 – 27 September 2013
Holiday Villa Beach Resort & Spa, Langkawi, Malaysia

Organized by
Electron Devices Chapter of IEEE Malaysia Section

Co-organized by
Institute of Advanced Technology (ITMA),
Universiti Putra Malaysia

School of Microelectronics Engineering,
Universiti Malaysia Perlis



IEEE-RSM 2013 Committee

Advisor:

Prof. Dato' Dr. Burhanuddin Yeop Majlis *Universiti Kebangsaan Malaysia*

Chair:

Assoc. Prof. Dr. Mohd Nizar Hamidon *Universiti Putra Malaysia*

Co-Chair:

Assoc. Prof. Dr. Roslina Mohd. Sidek *Universiti Putra Malaysia*

Technical Chair:

Assoc. Prof. Dr. Badariah Bais *Universiti Kebangsaan Malaysia*

Hon. Secretary:

Assoc. Prof. Dr. P. Susthitha Menon *Universiti Kebangsaan Malaysia*

Treasurer:

Mr. Azrif Manut *Universiti Teknologi MARA*

Local Arrangement Chair:

Assoc. Prof. Dr. Zaliman Sauli *Universiti Malaysia Perlis*

Publicity Chairs:

Dr. Zubaida Yusoff *Multimedia University*
Pn. Maizatul Zolkapli *Universiti Teknologi MARA*

Committee Member

Prof. Dr. Muhammad Mat Salleh *Universiti Kebangsaan Malaysia*
Prof. Dr. Uda Hashim *Universiti Malaysia Perlis*
Prof. Dr. Ibrahim Ahmad *Universiti Tenaga Nasional*
Prof. Dr. Razali Ismail *Universiti Teknologi Malaysia*
Prof. Dr. Othman Sidek *Universiti Sains Malaysia*
Prof. Dr. A.H.M Zahirul Alam *International Islamic University Malaysia*
Assoc. Prof. Dr. Nafarizal Nayan *Universiti Tun Hussein Onn*
Assoc. Prof. Dr. Azlan Abdul Aziz *Universiti Sains Malaysia*
Assoc. Prof. Dr. Norhayati Soin *Universiti Malaya*
Dr. Zainal Arif Burhanudin *Universiti Teknologi Petronas*
Ir. Nor Azhadi Ngah *TMR&D Sdn. Bhd.*
Dr. Ismail Saad *Universiti Malaysia Sabah*
Dr. Wan Zuha Wan Hasan *Universiti Putra Malaysia*
Dr. Asrulnizam Abdul Manaf *Universiti Sains Malaysia*
Mr. Hazian Mamat *MIMOS Berhad*

Secretariat

Encik Md Ali Rani
Puan Rosiah Osman
Puan Intan Helina Hassan
Puan Aishah Fauthan
Cik Sri Vanitha Mathy

Secretariat Office

Secretariat of IEEE-RSM 2013
Electron Devices Malaysia Chapter
Institute of Advanced Technology (ITMA)
Universiti Putra Malaysia, 43400 UPM Serdang, Selangor, MALAYSIA
Telephone +603 8946 8475/8464/7557
Fax +603 8946 7006
Email: edsmalaysia@gmail.com



Keynote

No.	Title	Pages
K01.	Low Power Green Electronic Devices	i
K02.	Silicon Photonics for Microelectronic Op-Chip Optical Interconnects	ii
K03.	Fabrication and Characterization of Polysilicon Nanogap Device for DNA Hybridization Detection	iii
K04.	An Overview of Innovation Ecosystem in Malaysia	iv
K05.	Analysis Challenges and Interface Physics in Silicon Nanodevices	v
K06.	Artificial Pinning Centers for Superconducting Microwave Resonators	vi
K07.	MEMS and Lab on Chip: Interfacing Macro to Nano World	vii

MEMS and Microsensors

No.	Title	Pages
001.	Finite Element Modeling of SAW Resonator in CMOS Technology for Single and Double Interdigitated Electrode (IDT) Structure	1
002.	Fabrication of the Trapezoidal Electrodes and Electrets Material for Electrostatic Energy Harvester	5
003.	Design of CMOS-MEMS Based Thermoelectric Generator	9
004.	Characterization of Unipolar Nanorectifiers Coupled with an RF Antenna	13
005.	Photoresist Microbridge Pattern Optimization at 1 μ m using Conventional Photolithography Technique	17
006.	Design and Optimization of Magnetic Particles Embedded In PDMS Membrane	21
007.	Finite Element Analysis on Magnetic Force Generation of Electromagnetic Microactuator for Micropump	25
008.	Fabrication and Characterization of Metal Microwire Transducer for Biochip Application	29
009.	pH Measurement using In House Fabricated Interdigitated Capacitive Transducer	33
010.	A Novel of Fluidic Based One Side Electrode Type Pressure Sensor	37

011.	Design and Analysis of a Low-Voltage Electrostatic Actuated RF CMOS-MEMS Switch	41
012.	Design and Simulation of 20MHz Oscillator using CMOS-MEMS Beam Resonators	45
013.	Characterization Direct Bonding of SiC/SiN Layer on Si Wafer for MEMS Capacitive Pressure Sensor	50
014.	Quantitative Measurement of Sugar Concentration using In House Fabricated Microgap Biosensor	54
015.	A Novel Tunable Water-Based RF MEMS Solenoid Inductor	58
016.	Centered-Gap and Aligned-Gap Multiple Split Ring Resonator for Bio-Sensing Application	62
017.	Ni ₈₀ Fe ₂₀ V-Shaped Magnetic Core for High Performance MEMS Sensors and Actuators	66
018.	Analytical Modeling and Simulation of a CMOS-MEMS Cantilever Based CO ₂ Sensor for Medical Applications	70
019.	Pressure Distribution Characterization in Forward Facing Step (FFS) Microchannel using Ansys	74
020.	Annealing Effects on Structural and Electrical Properties of Micro Heater Conductor Element	77

Circuit, VLSI & Microwave

No.	Title	Pages
021.	Memristor Based Delay Element using Current Starved Inverter	81
022.	Determination of Pulverized Material Permittivity for Microwave Absorber Application	85
023.	A Simulation Study of Thickness Effect in Performance of Double Lateral Gate Junctionless Transistors	89
024.	A Low Voltage Low Power 3.5/5.8 GHz Dual-Band Common Gate Low Noise Amplifier	93
025.	Effect of Source-Drain Metal Shield in FET Structure on Drain Leakage Current	97
026.	Numerical Investigation of Channel Width Variation in Junctionless Transistors Performance	101

027.	Design and Analysis of a Wireless Temperature Monitoring System	105
028.	0.35 μ m SPDT RF CMOS Switch for Wireless Communication Application	109
029.	15 GHz Medium Power Amplifier Design Based On 0.15 μ m p-HEMT GaAs Technology For Wideband Applications	113
030.	Modeling and Simulation of Microscopic Defects in CIS-based Solar Cell Thin Film using Silvaco TCAD	117
031.	Parametric Analysis for Designing Low Voltage and Low Frequency Energy Harvester Booster	122
032.	Threshold Voltage Optimization in a 22nm High-k/Salicide PMOS Device	126
033.	Effect of Channel Width-to-Length Ratio on Isothermal Point of MOSFET-ISFET Structure	130
034.	Schottky Contact in P-HEMT Wafer using Metallization with Ge/Au/Ni/Au	134
035.	Design of CMOS based Programmable Gain Operational Amplifier	139
036.	Calibration of the Density-Gradient TCAD Model for Germanium FinFETs	143
037.	Emulation of Double Gate Transistor in Ultra-Thin Body with Thin Buried Oxide SOI MOSFETs	147
038.	Frequency Dependence of Quality Factor in Vibration Energy Harvesting	151

Materials & Devices

No.	Title	Pages
039.	Effect of Film Thickness on the Memristive Behavior of Spin Coated Titanium Dioxide Thin Films	155
040.	Annealing Effects on Titanium Dioxide Films by Sol-Gel Spin Coating Method	159
041.	Effect of RF Sputtered Arc-TiO ₂ and Sol-Gel c-TiO ₂ Compact Layers on The Performance of Dye-Sensitized Solar Cell	163
042.	Effects of Annealing Temperature on Current-Voltage Characteristics of TiO ₂ Thin Film by Sol-Gel Process on Silicon Substrate for Biosensor Application	167
043.	Influence of Metal Catalyst for Zinc Oxide Nanostructures Grown by TCVD Method for Extended-Gate FET Sensor Application	171

044.	Acoustic Wavelength Effects on the Propagation of SAW on Piezo-Crystal and Polymer Substrates	175
045.	Effect of [6,6]-Phenyl-C ₆₁ Butyric Acid Methyl Ester (PCBM) Agglomerated Nanostructure on Device Performance in Organic Thin-Film Transistors	179
046.	Electrical and Structural Characterization of Zn Doped CuGaO ₂ Films	183
047.	High Power LED Heat Dissipation Analysis Using Cylindrical Al Based Slug using Ansys	186

Materials & Process

No.	Title	Pages
048.	Analysis on Electrical and Optical Properties of Nitrogen Incorporated Amorphous Carbon Prepared by Aerosol-Assisted CVD Method	190
049.	Highly Sensitive Porous PtSi/Si UV Detector with High Selectivity	194
050.	Dielectric Property of Lead Titanate Thin Films Prepared on Glass Substrate at Low Temperature	197
051.	The Effect of Phosphate Buffer Solution (PBS) Concentration on the Ion Sensitive Field-Effect Transistor (ISFET) Detection	200
052.	Fabrication of Silicon Nitride Ion Sensitive Field- Effect Transistor (ISFET)	204
053.	Structural Characterization of Zinc Oxide Thin Films Deposited at Various O ₂ /Ar Flow Ratio in Magnetron Sputtering Plasma	208
054.	Fabrication of Poly-Silicon Microwire using Conventional Photolithography Technique: Positive Resist Mask vs Aluminum Hard Mask	211
055.	Two-Stage MMIC Medium Power Amplifier using Depletion Mode PHEMT for 5.8GHz Applications	215
056.	Sputtered Titanium Dioxide Thin Film for Extended-Gate FET Sensor Application	219
057.	The Study on the Aspect Ratio of Atomic Force Microscope (AFM) Measurements for Triangular Silicon Nanowire	223
058.	Effect of Annealing Temperature on Electrical and Optical Properties of ZnO Thin Films Prepared by Sol Gel Method	227
059.	Impact of Processing Parameters on Low-Voltage Power MOSFET Threshold Voltage Considering Defect Generation	231

060.	Nitrogenated Amorphous Carbon Film by Thermal Chemical Vapor Deposition	235
061.	Wettability Analysis on Platinum Deposited Wafer After Reactive Ion Etching Using SF ₆ +Argon Gaseous	239
062.	Main Factor Interaction Relationship of Lattice Parameter in Ba _{0.65} Sr _{0.35} TiO ₃ Thin Films Processing	242
063.	Ba _{0.7} Sr _{0.3} TiO ₃ Thin Film Dielectric Properties with Different Deposition Layer	245

Photonics

No.	Title	Pages
064.	Four Wave Mixing and Cross Gain Modulation Wavelength Converters in Semiconductor Optical Amplifier	248
065.	Surface Roughness Analysis on Platinum Deposited Wafer after Reactive Ion Etching Using SF ₆ +Argon/CF ₄ +Argon Gaseous	251
066.	Responsivity Optimization of a MQW SOI-based Lateral PIN Photodiode using Taguchi's L ₂₇ Orthogonal Array	254
067.	Photoanode of Nanostructured TiO ₂ Prepared by Ultrasonic Irradiation Assisted of Sol-Gel with P-25 for Dye-Sensitized Solar Cells	258
068.	Effect of Anatase TiO ₂ Overlayer on the Photovoltaic Properties of Rutile Phase Nanostructured Dye-Sensitized Solar Cell	262
069.	Electroluminescence Behavior of MEH-PPV Based Organic Light Emitting Diode	265
070.	Simulation of Mach Zehnder Interleaver Based Thermo-Optic Effect in L-Band Range	269
071.	High Density Printing Paper Quality Investigation	273

Nanotechnology

No.	Title	Pages
072.	Mechanical Milling of Tronoh Silica Sand Nanoparticles using Low Speed Ball Milling Process	278

073. Humidity Sensor Based on SnO ₂ Nanoparticle Thin Film Synthesized by Thermal Chemical Vapor Deposition (CVD)	281
074. Improvement in Dielectric Properties of Bilayer ZnO/MgO Films Deposited by Sol-Gel Technique	285
075. Capacitance-Voltage Hysteresis of MIS Device with PMMA: TiO ₂ Nanocomposite as Gate Dielectric	289
076. Effect of Nitrogen Concentrations on Electrical Properties of Amorphous Carbon Thin Films by Using Palm Oil Precursor	293
077. Fabrication of Nanodiodes using Atomic-Force Microscope Lithography	297
078. The Properties of P-type Copper (I) Iodide (CuI) as a Hole Conductor for Solid-State Dye Sensitized Solar Cells	300
079. Investigating the Annealing Effect on the Conventional Growth of ZnO Nanorod Through Electrical Characterization	304
080. Structural Properties of Al-doped ZnO Thin Films Deposited by Sol-Gel Spin-Coating Method	308
081. Iodine doped Multiwall Carbon Nanotubes in MEH-PPV:I-MWCNTs Nanocomposite for Organic Solar Cell Applications	312
082. Fabrication of Multi-walled Carbon Nanotubes Hydrogen Sensor on Plastic	316
083. Single and Dual Strained Channel Analysis of Vertical Strained- SiGe Impact Ionization MOSFET (VESIMOS)	320
084. The Effect of Width on Graphene Nanoribbon Density of State Under Uniaxial Strain	324
085. Spherical to Polyhedral Pt Nanocrystal Formation Assisted with Methylamine	328
086. Schottky Barrier Lowering Effect on Graphene Nanoribbon Based Schottky Diode	332
087. Body Doping Analysis of Vertical Strained-SiGe Impact Ionization MOSFET Incorporating Dielectric Pocket (VESIMOS-DP)	336
088. Hybrid Organic-Inorganic Light Emitting Diode using ZnO Nanorods as Electron Transport Layer	340
089. Hydrothermal Synthesis of TiO ₂ Nanostructures On Pre-treated Substrate	344
090. High Frequency Small Signal Modeling of CNTFET	348

091.	Morphology, Topography and Thickness of Copper Oxide Thin Films Deposited using Magnetron Sputtering Technique	352
092.	Physical Properties of Tin Oxide Thin Films Deposited using Magnetron Sputtering Technique	356
093.	Effect of Catalyst on the Fluorescence Quenching of [Tris (4, 7-Diphenyl-1, 10-Phenanthroline) Ruthenium (II) Dichloride] for Dissolved Oxygen Detection	360
094.	Growth of Multi-walled Carbon Nanotubes on Platinum	363
095.	Lithography Method for Selective Area CNTs Growth	367
096.	Hysteresis Behaviour of Top-Down Fabricated ZnO Nanowire Transistors	371

Others

No.	Title	Pages
097.	FIB with EDX Analysis use for Thin Film Contamination Layer Inspection	375
098.	Design Optimization of MEMS Dual-Leg Shaped Piezoresistive Microcantilever	379
099.	Design and Simulation of Piezoelectric Micro Power Harvester for Capturing Acoustic Vibrations	383
100.	3D Electromagnetic Simulation of Interconnect Fault Inspection Based on Magnetic Field Behavior	387
101.	Effect of Microchannel Geometry in Fluid Flow for PDMS Based Device	391
102.	A Sensitivity Study of Piezoresistive Pressure Sensor for Robotic Hand	394
103.	Numerical Study of Side Gate Junction-less Transistor in On State	398
104.	Effect of TiO ₂ Nanostructure's Shape on the DSSCs Performance	402
105.	Effects of TiO ₂ Electrode Thickness on the Performance of Dye Solar Cell by Simulation	406
106.	Double Gate Junctionless MOSFET Simulation and Comparison with Analytical Model	410
	Index	414

Simulation of Mach Zehnder Interleaver Based Thermo-Optic Effect in L-Band Range

Ratih Retno Palupi¹, Ary Syahriar¹, Ahmad H. Lubis¹, Sasono Rahardjo², Sardjono²

¹Department of Electrical Engineering, University of Al Azhar Indonesia

²The Agency for the Assessment and Application of Technology
Jakarta, Indonesia

ratihpalupi@live.com, ary@uai.ac.id, sasono@gmail.com

Abstract—Optical device based on Mach Zehnder Interferometer (MZI) is usually used as the optical switching, modulator and many applications in telecommunication networks. This paper discuss the Temperature Effect of Wavelength Division Multiplexing (WDM) Interleaver by using single and cascaded MZI. The Sellmeier equation is used to calculate the refractive index changing caused by the temperature changing. The output power of MZI is obtained by using matrix equation. The characteristic of output power varied with several temperatures between 28 and 300 degree Celsius. The wavelength used in this simulation is in L-Band region which is about 1570-1610nm. Temperature changing cause the changing of refractive index of material. The temperature changing leads to the shifting of wavelength channel which describe the characteristic of thermo optic effect on single and cascaded MZI.

Keywords—single and cascaded Mach Zehnder Interferometer; Thermo-optic effect; Sellmeier Equation; transfer matrix method; wavelength shift.

I. INTRODUCTION

Dense Wavelength Division Multiplexing (DWDM) is one of critical technology to enabling the capacity expansion of fiber optic which can exponentially increase the bandwidth of optical communication. One of optical device that can be classified as optical wavelength circuit for WDM communication is the Mach Zehnder Interferometer (MZI). The MZI can be designed as optical passive component such as switches[1], interleaver[2][3], add-drop filters[4], modulator and demodulator[5] etc.

One popular technological issue is related with the capability to perform optical modulation and one of the interesting way to modulate the refractive index in silica waveguide is by using the thermo-optic effect. This effect is allowing low transmission loss, low cost, high stability, low power consumption, and very large scale of integration[6].

The thermo-optic effect on Cascaded Mach Zehnder Interleaver is explained by using sellmeier coefficient to obtain the changing of refractive index of silica which will discussed in part II, and the matrix equation is needed to calculate the output power of MZI and Comparison result of the thermo-optic effect on single and cascaded MZI is the important part to be discussed.

II. TEMPERATURE EFFECT IN REFRACTIVE INDEX OF SILICA

Silica waveguides is one of the material that usually used in optical device because this material has several advantages, including: low propagation loss, low coupling loss and reflection, excellent physical and chemical stability, low cost and large scale and also it is easy to control the phase by using thermo-optic effect.

The thermo-optic effect is a phenomenon by which the refractive index of a substance changes with temperature [9]. In silica glass, this effect is characterized by an increase in the refractive index as the temperature rises.

The sellmeier equation is an equation to characterize the heating effect in material. The sellmeier coefficients at any temperature T are computed from the room temperature and the thermo optic-coefficient (dn/dT) of material, where the thermo-optic coefficient for silica is $10^{-5} (^{\circ}\text{C}^{-1})$ [7]. The new effective refractive index due to temperature can be calculated by using the equation below[7].

$$n_T = n_R + (T - R) (dn/dT) \quad (1)$$

By using Eq.(1) the relation of refractive index as a function of temperature can be simulated in Fig.1. The refractive index is increased linearly with the increasing of temperature. It is because the rising temperature cause the electrons of material move faster, so that the refractive index of material is increased.

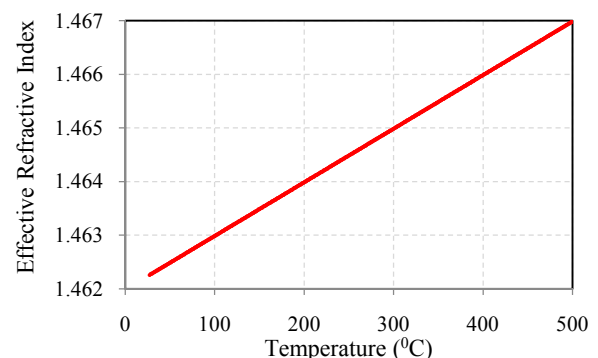


Fig 1. Effective refractive index as a function of temperature

III. MACH ZEHNDER INTERLEAVER

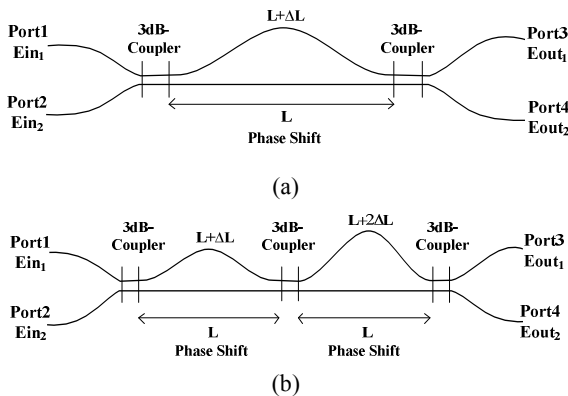


Fig. 2. MZI Structure (a) Single MZI, (b) Cascaded MZI

The MZI modulator has been extensively investigated and reported in the literature since 1980's as a potential electro-optic modulator for high digital bit-rate and RF transmission over optical fiber communication systems[8].

A. Single Mach Zehnder Interferometer(MZI)

The single MZI structure is consist of two 3dB silica directional coupler connected by two guide arms. The first coupler has function as a splitter and the second coupler as a combiner.

The transmission characteristic of MZI can be described using matrix method. The propagation matrix $M_{coupler}$ is described by [9]:

$$M_{coupler} = \begin{bmatrix} \cos \theta & j \sin \theta \\ j \sin \theta & \cos \theta \end{bmatrix} \quad (2)$$

Where $\theta = Kd$ and K is coupling coefficient and d is coupling length, since the 3dB couplers MZI divide the power in equal rate, therefore $2Kd = \pi/4$.

In the central region the signals which entering the arms is coming from the same light source, the output from this two guides have a phase difference $\Delta\phi$, the propagation matrix $M_{\Delta\phi}$ for the phase shifter is:

$$M_{\Delta\phi} = \begin{bmatrix} e^{j\beta\Delta L} & 0 \\ 0 & e^{-j\beta\Delta L} \end{bmatrix} \quad (3)$$

$\beta = 2\pi n_{eff}/\lambda$ is the propagation constant, n_{eff} is effective refractive index dan ΔL is the arm's length difference. The relation between the output optical fields $E_{out,1}$ and $E_{out,2}$ with the input fields $E_{in,1}$ and $E_{in,2}$ is:

$$\begin{bmatrix} E_{out,1} \\ E_{out,2} \end{bmatrix} = M \begin{bmatrix} E_{in,1} \\ E_{in,2} \end{bmatrix} \quad (4)$$

Where: $M = M_{coupler1} \cdot M_{\Delta\phi} \cdot M_{coupler2}$ (5)

The propagation power of MZI is shown in Fig.3, and the parameters used in this calculation are: $n_1 = 1.464$, $n_2 = 1.458$ (n_1 , n_2 are the refractive index material in core and cladding,

respectively), waveguide core width $h = 7\mu\text{m}$, $\lambda = 1.570\mu\text{m} - 1.6\mu\text{m}$.

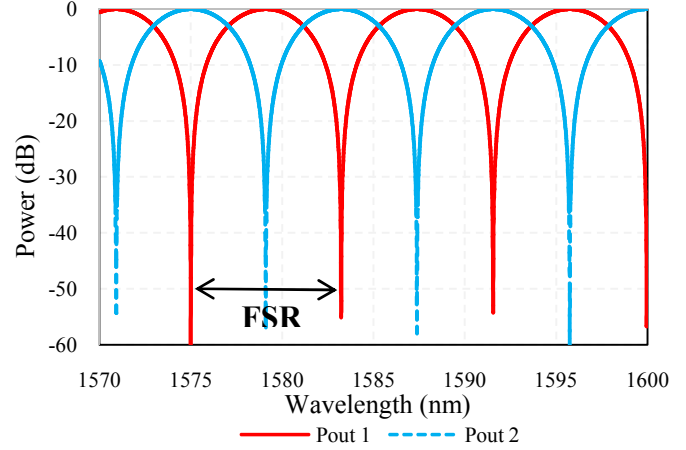


Fig. 3 Spectral response of single MZI

Fig. 3 shows that the MZI is a scalable device. This means that its spectral properties are periodic and these periodicities is called Free Spectral Range (FSR) [2]. This simulation shows the value of FSR is about 8,2 nm with the channel isolation power is less than -50dB in all wavelength range and the channel spacing between port1 and port2 is 4,08 nm.

B. Two-Stage Cascaded Mach Zehnder Interferometer

The following discussion observes the characteristic of Two-stage Cascaded Mach Zehnder Interferometer which consist of three 3-dB couplers and two phase shifter where $\Delta L_2 = 2\Delta L_1$. The Cascaded MZI shown in Fig.2 (b) has a spectral response with a wider bandwidth than a single MZI [11].

Using the same method derivation in Eqs.(2) to (5), The spectral response of cascaded MZI is simulated using the following parameters : $n_1 = 1.464$, $n_2 = 1.458$ (refractive index in core and cladding), $\lambda_0 = 1575\text{nm}$ (central wavelength), $h = 7\mu\text{m}$ (core width), $\Delta L = 103.4\mu\text{m}$ (arm's length difference) and L-Band wavelength range (1575-1600nm).

The spectral response of cascaded MZI is shown in Fig.4. The isolation power, crosstalk power, and FSR value from Fig.4 is summarized in Table 1.

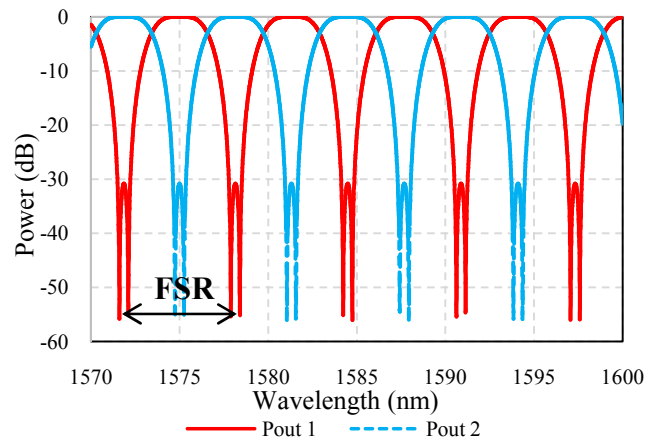


Fig. 4. Spectral response of cascaded MZI

TABLE I
CHARACTERISTIC OF CASCADED MACH ZEHNDER INTERFEROMETER

NO	Result	Value
1.	Isolation Power	-55dB
2.	Crosstalk	-30dB
3.	Channel Spacing	0,0082μm
4.	Space between Port1 and Port2	4,13nm

From simulation in Fig. 3 and 4, and Table1 shows the channel spacing of single and cascaded MZI is matching to the channel spacing of 100GHz L-Band ITU grid DWDM specification which is possible to all WDM channel.

IV. THERMO-OPTIC EFFECT ON MACH ZEHNDER INTERLEAVER

By using sellmeier equation, the changed of effective refractive index due to temperature had been explained in Fig.1. Since temperature is affecting to refractive index, then the propagation constants β is also depend on temperature. It is mean that the transmission power of MZI is influenced by the temperature change.

A. Temperature Effect on Single MZI

The spectral response of single MZI is shown in Fig.5, The parameters used in this simulation are: $n_1=1.464$, $n_2=1.458$, $\lambda=1570\text{nm}-1600\text{nm}$, $h = 7\mu\text{m}$ and $\Delta L = 103.4\mu\text{m}$.

The spectral responses are simulated in several temperatures with $\Delta T=100^\circ\text{C}$. The characteristic of single MZI which is shown in Fig.5 are summarized in Table 2.

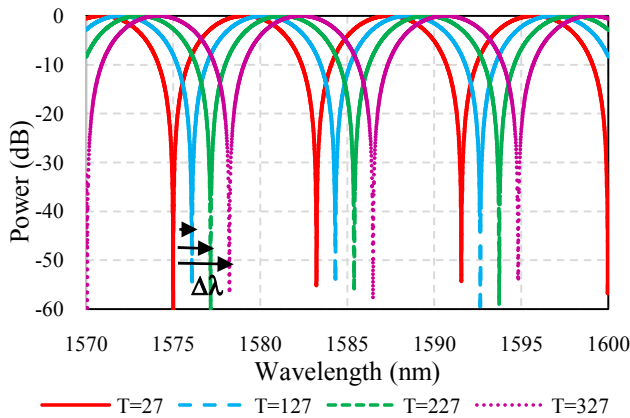


Fig. 5 Spectral response of single MZI in several temperature

TABLE 2
CHARACTERISTIC OF SINGLE MACH ZEHNDER INTERFEROMETER IN SEVERAL TEMPERATURE

No	Result	T_R	$T_1=127$	$T_2=227$	$T_3=327$
1.	Power	<-55dB	<-55dB	<-55dB	<-55dB
2.	FSR	8,2nm	8,2nm	8,2nm	8,2nm
3.	Wavelength Shift ($\Delta\lambda$)		1,08nm	2,15nm	3,23nm

B. Temperature Effect on Cascaded MZI

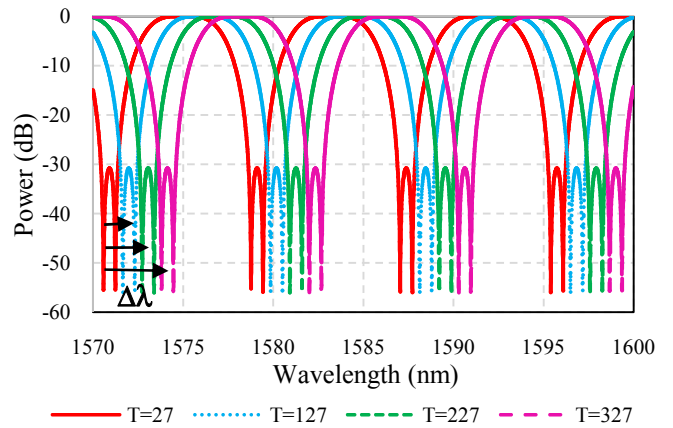


Fig.6 Spectral response of cascaded MZI in several temperature

Fig.6 shows the spectral response of cascaded MZI in temperature $T=27^\circ\text{C}$, 127°C , 227°C , 327°C . For simplicity, the temperature is notated as T_R , T_1 , T_2 , and T_3 respectively. The result of Fig.6 are summarized in Table 3.

A. Wavelength Shifting caused by Temperature Changing

Figs. 5, 6 and Tables 2, 3 shows that the heating in single and cascaded MZI is affecting to the wavelength shift. Simulation result from Table 2 and Table 3 shows that the wavelength shift in single and cascaded MZI has the same value. The relation of wavelength shift as a function of temperature changing is shown in Fig.7.

TABLE 3
CHARACTERISTIC OF CASCADED MACH ZEHNDER INTERFEROMETER IN SEVERAL TEMPERATURE

No	Result	T_R	T_1	T_2	T_3
1.	Isolation Power	-55dB	-55dB	-55dB	-55dB
2.	Crosstalk	-30dB	-30dB	-30dB	-30dB
3.	Channel Spacing/FSR	8,2nm	8,2nm	8,2nm	8,2nm
4.	Wavelength Shift ($\Delta\lambda$)		1,08nm	2,15nm	3,23nm

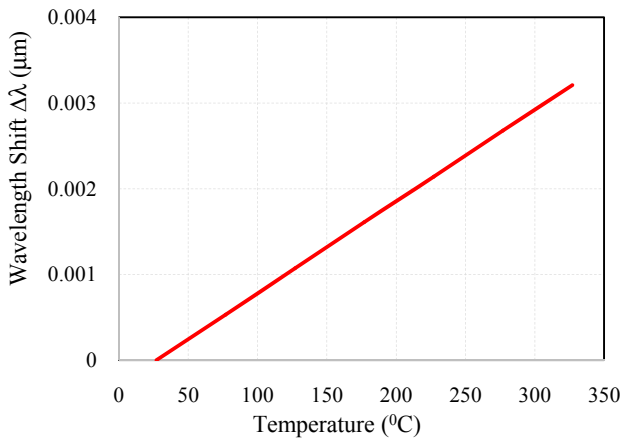


Fig. 7 Wavelength shift as a Function of Temperature

Fig.7 shows that the higher temperature produce the wider wavelength shifting. To describe the relation between wavelength shift and temperature changing, we use brute forces to fit a linear equation into λ shifting data caused by the temperature effects, which results in the following equation:

$$\lambda_T = \lambda_R + [1.08(T - T_R)](10^{-5}) \quad (6)$$

Where λ_R and λ_T are wavelength at room, and T is temperature, respectively. Wavelength shift ($\Delta\lambda$) is $\Delta\lambda = \lambda_R - \lambda_T$ (μm), T and T_R are temperature at room and T ($^{\circ}\text{C}$) and 1.08×10^{-5} is constant. In designing an interleaver based thermo-optic, this equation can be used to immediately find out how many degrees the temperature should be heated to obtain a particular wavelength shift.

V. CONCLUSION

From simulation and discussion it can be concluded that the heating effect on single and cascaded MZI cause the

wavelength shift. The value of wavelength shift due to temperature can be calculated by applying Eq.(6). This equation can be used as a basis for designing the MZI based thermo-optic, to obtain the degrees of temperature should be heated to produce a certain wavelength shift.

REFERENCES

- [1]. D. Agifral, A. Syahriar, A.H. Lubis, "Simulation of Optical Switching Based on Mach Zehnder Interferometer Structure", IEEE 978-1-4244-5586-7, 2010.
- [2]. Schewlb. Otto, "Cascaded Mach-Zehnder Interleaver Networks for WDM Systems". An Internal Report for OTKA Project T.026277, April 2005.
- [3]. B. J. Offrein, G. L. Bona, F. Horst, H. W. M. Salemink, R. Bayeler, and R. Germann, "Wavelength Tunable Optical Add-Drop Filter with Flat Passband for WDM Networks", IEEE Photonics Technology Letters, Vol.11, No.2, February 1999.
- [4]. Huai-Wei Lu, Kai-jun Wu, Yun Wei, Bao-Ge Zhang, Guan-Wei Luo, "Study of All-Fiber Assymmetric Interleaver Based on Two Stage Cascaded Mach Zehnder Interferometer", Elsevier Journal Optical Communication 285 (2012) 1118-1122.
- [5]. Y. Nasu, K. Hattori, T. Saida, Y. Hashizume, Y. Sakamaki, "Silica-Based Adaptive-Delay DPSK Demodulator with Cascaded Mach-Zehnder Interferometer Configuration". ECOC 2010, 19-23 September, Torino, Italy.
- [6]. Francesca Magno, Francesco Dell'Olio and Vittorio M.N. Passaro, "Multiphysics Investigating of Thermo-Optic Effect in Silicon-On-Insulator Waveguide Arrays", Proceeding of the COMSOL Users Conference, Milano : 2006.
- [7]. Bradley J. Frey, Douglas B. Leviton, Timothy J. Modison, "Temperature-dependent refractive index of silicon and germanium", NASA Goddard Space Flight Center, Greenbelt, MD 2077.
- [8]. LN Binh, Itzhak Shraga, "An Optical Fiber Dispersion Measurement Technique and Systems", Department of Electrical and Computer Systems Engineering Monash University, 2005
- [9]. Esmael M. Yahya, "Mach Zehnder Interferometer", Universiti Teknologi Malaysia, Malaysia, 2007.
- [10]. Maria L. Calvo and Vasudevan Lakshminarayanan, "Optical Waveguide From Theory to the Applied Technology", CRC Press : New York 2007
- [11]. Qian Wuang, Sailing He, "Optical Design Of A Flat-Top Interleaver Based On Cascaded Mzi By Using A Genetic Algorithm", Elsevier journal, 2003.